SSRG International Journal of Electrical and Electronics Engineering
ISSN: 2348-8379/ https://doi.org/10.14445/23488379/IJEEE-V11I6P126

Volume 11 Issue 6, 242-249, June 2024
© 2024 Seventh Sense Research Group®

Original Article

A Novel Control for Partial Power Charging Circuit Topology with Fast EV Charging Application

Challa Ramaiah[1], Edara Venkata Chandra Sekhara Rao[2], Satish Kumar Peddapelli[3]

[1]*Department of Electrical Engineering, Osmania University, Telangana, India.*
[2]*Departments of Electrical and Electronics Engineering, MVSR Engineering College, Telangana, India.*
[3]*Department of Electrical Engineering, Osmania University, Telangana, India.*

[1]*Corresponding Author : challaramu9@gmail.com*

Received: 12 April 2024 Revised: 14 May 2024 Accepted: 12 June 2024 Published: 29 June 2024

Abstract *- Conventional circuits for EV battery charging have lower ratings, which can charge the batteries at lower currents. This causes a long wait time to charge heavy EV batteries becoming a greater drawback to the EV sector. Fast charging circuits need to be deployed to charge the EV batteries with higher charging current ratings. In this paper, a novel PPC circuit is introduced for fast charging of EV batteries using a high-frequency operated full bridge. The PPC circuit charged individual EV batteries with only processing of a fraction battery's total power. The proposed circuit is controlled with CC/CV control as per the SOC of the battery, retaining the health of the battery. The CC/CV control of the PPC circuit is designed with duty ratio control of the high-frequency full bridge. The duty ratio of the switches in the full bridge is controlled by the conventional PI gain controller with error generated by comparison of reference and measured values. The conventional PI controller is further updated with the PR controller, and a comparative analysis is done with dynamic conditions. A test module is designed with a PPC circuit connected to SST to a high voltage distribution line, charging a heavy EV battery. The comparative analysis is carried out in a Simulink environment of MATLAB software with graphical plotting done with respect to time.*

Keywords *- EV (Electric Vehicle), PPC (Partial Power Charging), CC (Constant Current), CV (Constant Voltage), SOC (State Of Charge), PI (Proportional Integral), PR (Proportional Resonant), SST (Solid State Transformer).*

1. Introduction

Transportation vehicles with Internal Combustion (IC) engines contribute to 30% of the global Carbon Dioxide (CO_2) emissions. Without measures to restrict the use of IC engine vehicles, this percentage may increase in the future. This heavy carbon footprint is leading to natural disasters and creating inhabitable conditions for humans and other living beings. To decarbonize transportation, IC engine vehicles need to be replaced with Electric Vehicles (EVs) [1].

EVs are powered solely by electricity from a high-capacity mobile battery pack. An electric motor drives the vehicle by drawing power from the battery pack. The battery pack needs to be charged later, either from a conventional power grid or renewable sources, depending on availability [2]. Previous research has shown that conventional charging methods, including buck, buck-boost, and PFC converters, have limited charging capability [3].

The converters' charge current prolongs the charging time, causing delays in transportation. Therefore, the charging current to the battery needs to be increased to enable faster charging. Fast charging stations are typically DC charging stations with powerful electronic circuits that can charge a battery with high currents. The power provided by fast-charging stations ranges from 10kW to 20kW. Using conventional circuit topologies to charge batteries in this power range can result in high ripple and disturbances, which can damage the battery pack. To address this, conventional converters are replaced with high-frequency full-bridge converters with High Frequency Transformers (HFTF) for better and faster charging of Electric Vehicles (EVs).

Additionally, for efficient power delivery and reduced size, a Solid-State Transformer (SST) is used instead of the conventional transformer. Each Power Processing Converter (PPC) circuit is connected to the SST to charge a single battery unit, using power partially from the mains. The system's structure is depicted in Figure 1, with the SST connected to a single-phase AC line at the distribution voltage level [6].

In Figure 1, the front-end converter connected to the 11kV MV grid distribution line converts AC to DC. The high-magnitude DC voltage is then input to the SST, which converts it to a low-magnitude DC voltage [7]. This is achieved by using two full bridges connected on the primary

This is an open access article under the CC BY-NC-ND license (http://creativecommons.org/licenses/by-nc-nd/4.0/)

and secondary sides of the HFTF. The HFTF has reduced turns on the secondary side, which decreases the voltage magnitude. The low-magnitude DC voltage after the second full bridge of the STT is the DC link of the system, where all the PPC circuits are connected. Each PPC circuit consumes partial power from the DC link for charging the EV and equally charges the battery packs connected in parallel [8]. This paper is organized with the proposed circuit topology and test system introduction in section 1, followed by the circuit configuration of the SST and PPC circuits in section 2 and also details the internal structure with power delivery and current paths of the circuits. Section 3 covers the design of the control structure that controls the PPC circuit, including CC/CV charging with respect to battery voltage. The design of the control structure with conventional PI and proposed PR controllers is included in section 3. Section 4 consists of a comparative analysis and validation of the results by simulating the proposed structure. The comparison is made between PI and PR CC/CV control with dynamic characteristics and references. The determination of the better-performing controller is validated in the conclusion of the paper in section 5, followed by references.

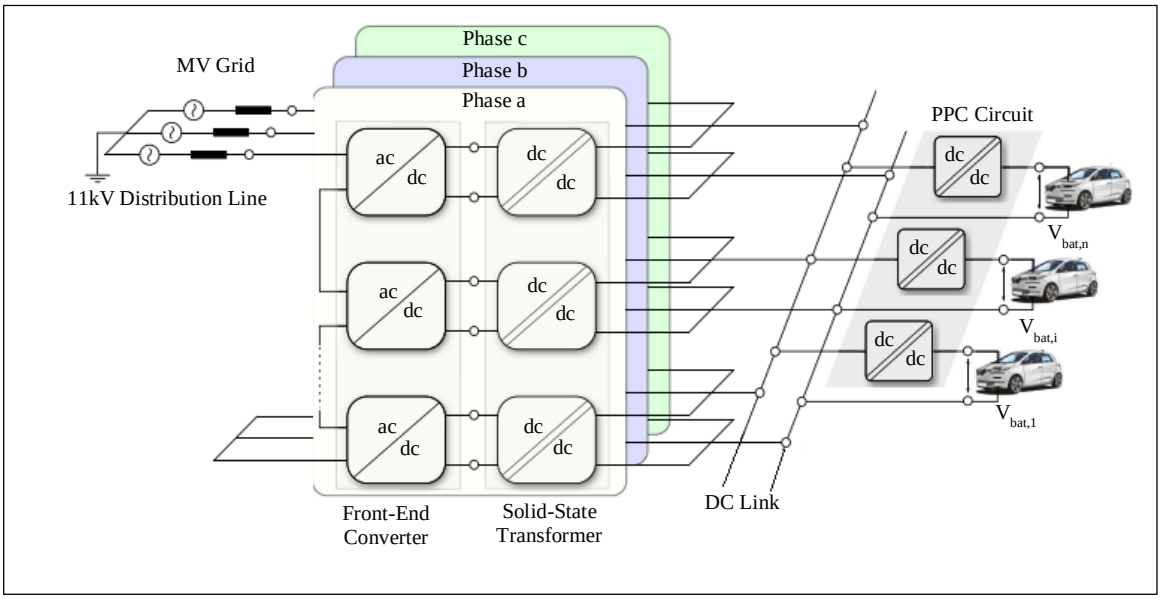

Fig. 1 Structure of the proposed system with SST and PPC circuits

2. Circuit Configuration

The circuit design being proposed replaces the traditional transformer with a power electronic-based step-down load transformer. This static transformer reduces the voltage levels to the range needed for charging Electric Vehicle (EV) batteries [9]. It consists of two full bridges connected on the primary and secondary of an HFTF. The DC voltage from a controlled rectifier connected to AC mains powers the primary full bridge, and after voltage step-down, the low magnitude DC voltage is sent to PPC circuits for charging EV batteries [10].

The PPC circuits ensure controlled charging of the EV battery using an active series-pass element, with very high efficiency and minimal power loss. The complete power from the DC link is transferred to the battery with very little loss. The PPC unit prevents circulating currents better than circuits with multiple charging units connected in parallel [11]. According to 'IEC 61851-23:2014', the voltage output ripple of the PPC circuit is maintained. Figure 2 shows the complete structure of the PPC circuit connected to the SST fed from the MV grid. The input is a single-phase AC voltage at a distribution voltage of 6.3kV and a fundamental frequency of 50Hz. The single-phase AC voltage (V_{ac}) is given as input to the controlled rectifier, which converts the AC voltage to high magnitude DC voltage ($V_{dc,cell}$) given as (1).

$$V_{dc,cell} = \sqrt{2}\,.V_{ac} \quad (1)$$

$$= 1.414 \text{ x } 6.3\text{kV} \cong 9\text{kVdc}$$

The 9kVdc is fed as input to the primary full bridge of the SST, converting it into high frequency AC in the range of 50-100 kHz. The high magnitude and high frequency AC voltage are induced to the secondary bridge through HFTF with a reduced turn's ratio for stepping down the voltage [12]. A HFTF is installed for reduced leakage currents and losses, increasing the efficiency of the SST. The secondary side full bridge converts the stepped down magnitude high frequency AC to low level DC voltage (V_{dc}) in the range of load consumption (300V-500V). These low voltages levels can be utilized for charging the EV battery or operating any DC load. Multiple PPC circuits are connected to this low-magnitude DC link for charging multiple EV batteries. The primary side of

HFTF in the PPC circuit is installed with a full bridge converting the low voltage DC to low voltage high frequency AC [13]. The high frequency AC is induced to the secondary side by the HFTF connected to an uncontrolled diode full bridge converting AC to DC, feeding the battery [14]. As per the given circuit configuration, battery voltage (V_{bat}) and V_{dc}, the PPC circuit can be operated in three different schemes, as in Figure 3.

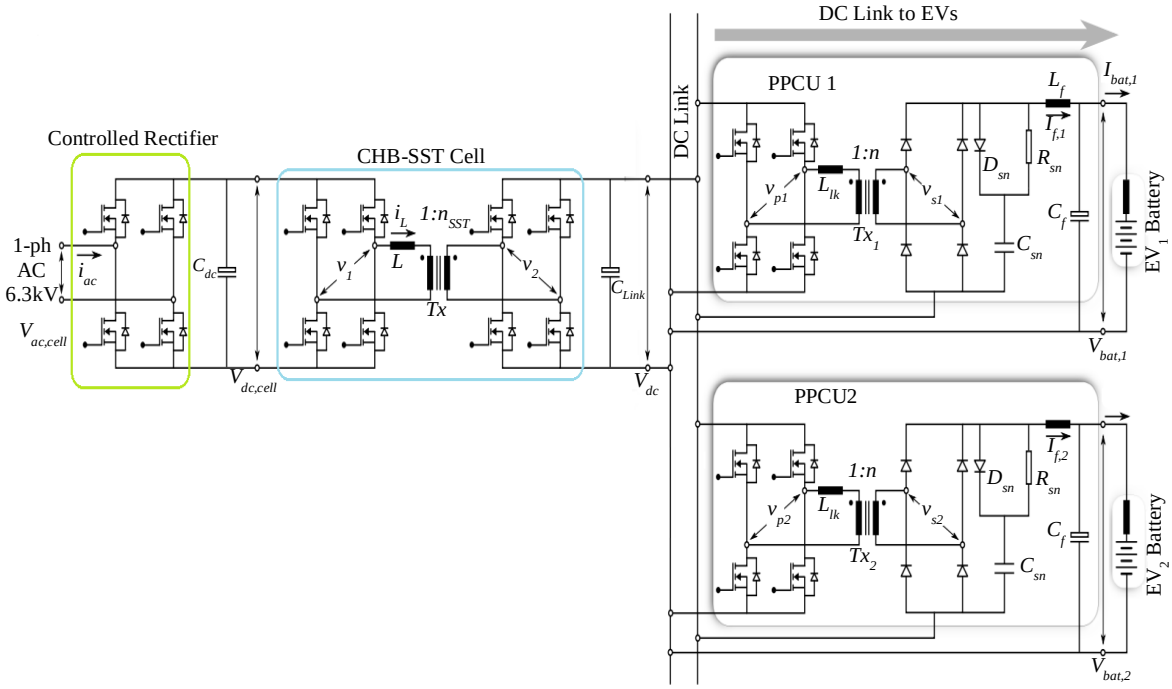

Fig. 2 Internal circuit structure of PPC circuit and SST

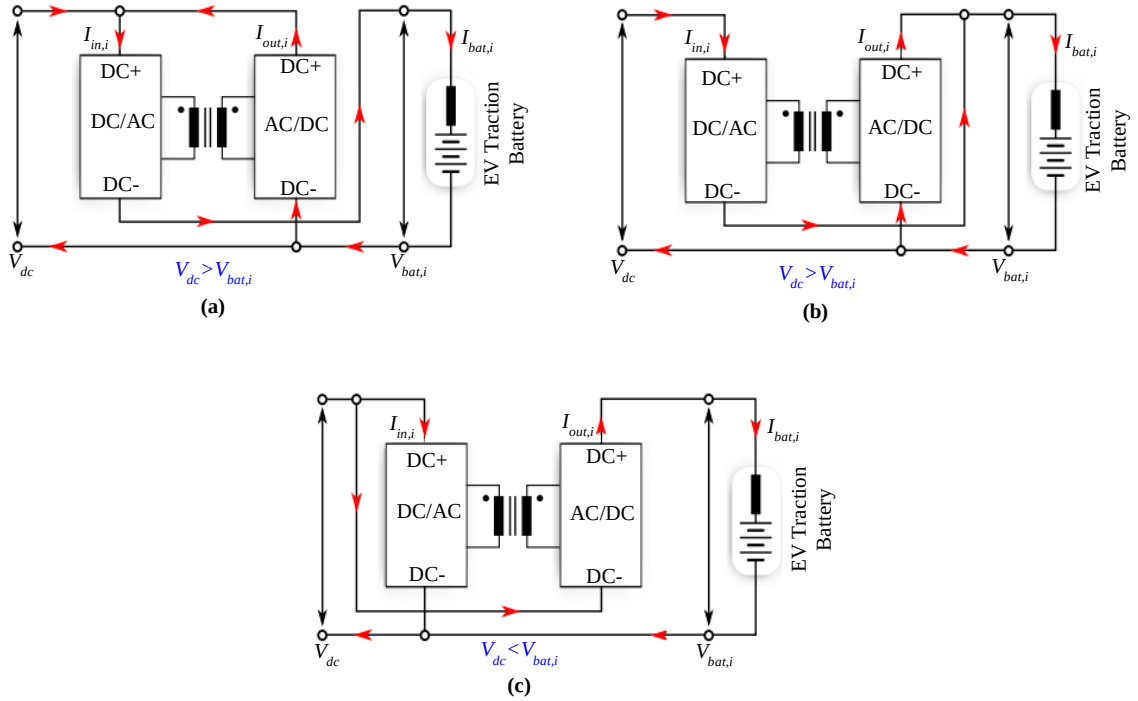

Fig. 3 (a) Scheme 1: $V_{dc} > V_{bat}$, (b) Scheme 2: $V_{dc} > V_{bat}$, and (c) $V_{dc} < V_{bat}$.

As per Figure 3, I_{in} is the input current to the primary bridge, I_{out} is the output current of the secondary bridge, I_{bat} is the charging battery current and variable 'i' represents the number of PPC circuit modules [15]. With respect to the type of scheme activated, the I_{bat} is expressed as follows:

$$I_{bat} = \begin{cases} I_{in} & (Scheme\ 1) \\ I_{in} + I_{out} & (Scheme\ 2) \\ I_{out} & (Scheme\ 3) \end{cases} \quad (2)$$

With Scheme 2, the battery can receive more charging current, achieving fast charging capability. As per the input power (P_{in}) and battery charging power (P_{bat}), the partiality ratio K_p is expressed as:

$$K_p = {P_{in}}/{P_{bat}} \quad (3)$$

As per Scheme 2, the input voltage and output voltage are variable, which can be controlled by changing the duty of the switches in the full bridge of the PPC circuit. The updated variables are expressed as:

$$V_{in} = V_{dc} - V_{bat} \quad (4)$$

$$V_{out} = V_{bat} \quad (5)$$

$$I_{in} = \frac{I_{bat}V_{bat}}{(1-\eta)V_{bat}+\eta V_{dc}} \quad (6)$$

$$I_{out} = \frac{\eta I_{bat}(V_{dc}-V_{bat})}{(1-\eta)V_{bat}+\eta V_{dc}} \quad (7)$$

$$K_p = \frac{V_{dc}-V_{bat}}{(1-\eta)V_{bat}+\eta V_{dc}} \quad (8)$$

Here, η is the efficiency of the PPC circuit given as:

$$\eta = {P_{bat}}/{(P_{bat} + P_{loss})} \quad (9)$$

The passive element ratings of the PPC circuit with respect to V_{dc}, V_{bat}, the duty cycle of switches (D) and sampling time (Ts) are given as follows:

$$L_f = \frac{(n.V_{dc}-(V_{bat}-V_{dc})).D.T_s}{\Delta I_f} \quad (10)$$

Here, ΔI_f is the allowable inductor current ripple, 'n' is the turns ratio of the HFTF in the PPC circuit given as:

$$n = {(V_{bat} - V_{dc})}/{D.V_{dc}} \quad (11)$$

Moreover, the maximum allowable duty ratio of the switches in the PPC circuit primary side is expressed as:

$$D = {\varphi_i}/{\pi} \quad (12)$$

Here, φ_i is the phase shift angle of the switching pulse fed to the switches. With the reduction of 'n' and 'D' values, the output voltage is also reduced, changing the charging current of the battery unit. As the 'n' remains constant in the HFTF once it is modelled, the only change that can be done is the dynamic 'D' value which varies the battery charging current [16]. The closed-loop design of the battery charge control is further explained in the next section.

3. Control Design

The control structure of the PPC circuit controls the battery charging current and the slope of the State-Of-Charge of the battery (SOC_{bat}). For fast charging of the battery the PPC circuit has to transfer more power to the particular battery pack [17]. The current to the battery needs to be limited as per the maximum withstanding charge current capacity of the battery. Every battery has its own limiting charging currents and voltage levels as per the manufacturing materials used for the fabrication of the battery [18].

As per previous research, the charging is categorized into two types: Constant Current (CC) and Constant Voltage (CV). The charging methods significantly control the charging of the battery as per the reference value specified. In CC mode, the reference is a current value (I_{ref}), and in CV mode, the reference is a voltage value (V_{ref}) [19]. The controlling modes are selected as per the battery voltage magnitude which changes as per the $\%SOC_{bat}$. The control structure design of the PPC circuit can be seen in Figure 4.

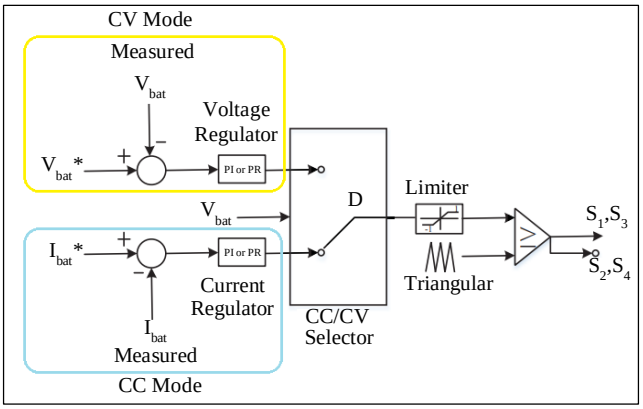

Fig. 4 CC/CV control modes of PPC circuit topology

In the selector switch, the switching happens by a threshold battery voltage value ($V_{batthres}$) set as per the $\%SOC_{bat}$. During lower $\%SOC_{bat}$ levels, the PPC circuit needs to be operated in CC mode for fast charging the battery pack with high power transfer. When the CC mode is selected, the current regulator (either PI or PR controller) generates D for the switches of the full bridge of the PPC circuit [20]. However, when the CV mode is selected, the voltage regulator generates the D value. The D signal is limited to a maximum of 48% (0.48), avoiding a short circuit of the PPC circuit. The D signal is now compared to high frequency triangular

waveform in the range of 50-100 kHz for the generation of pulses to the switches S1-S4. With the conventional PI regulator, the D value is expressed as:

$$D = (I^*_{bat} - I_{bat})\left(K_p + \frac{K_i}{s}\right) \quad (13)$$

Here, K_p and K_i are the proportional and integral gains tuned as per the response of the circuit topology. For better performance of the control structure, the conventional PI regulator is replaced with a PR controller with resonance gain replacing integral gain [21]. The new D signal with the PR regulator is expressed as:

$$D = (I^*_{bat} - I_{bat})\left(K_p + K_r \frac{2\omega_c s}{s^2+2w_c s+w_0^2}\right) \quad (14)$$

Here, K_r is resonant gain, ω_c is cut-off frequency and ω_0 is the resonant frequency. These values are updated as per the peak overshoot and settling time of the plant [22]. The modeling of the complete system is done with the two controllers performing a comparative analysis carried out in the next section.

4. Simulation Analysis

The modeling of the given circuit configuration of an EV fast charging station, including SST and PPC circuit charging a car EV battery, is done in a MATLAB Simulink environment. The blocks for the design are considered from the 'Powersystem' toolbox and 'Commonly used blocks' of the simulink library. The system configuration parameters considered for the modeling are given in Table 1.

Table 1. System parameters

Name of the Module	Parameters
Grid	Infinite Grid: 1-ph 6.3kV 50Hz
SST	f_{sst} = 50kHz, D_{sst} = 50%, HFTF: 10kVA, n = 22.5:1, L_m = 1mH.
PPC Circuit	f_{ppc} = 50kHz, $D_{max\text{-}ppc}$ = 48%, HFTF: 10kVA, n = 1:1, L_m = 695µH, C_{sn} = 49nF, R_{sn} = 500Ω, L_f = 520µH, C_f = 20µF.
EV Battery	Manufacturer: TATA Nexon (Basic) V_{nom} = 320V, Storage = 93Ahr
Controller	$V_{bat\text{-}ref}$ = 350V, $I_{bat\text{-}ref}$ = 20A, $K_{p\text{-}cv}$ = 0.05, $K_{i\text{-}cv}$ = 0.023, $K_{p\text{-}cc}$ = 0.5, $K_{i\text{-}cc}$ = 0.023. $K_{r\text{-}cv}$ = $K_{r\text{-}cc}$ = 0.05, w_o = 50Hz $V_{bat\text{-}threshold}$ = 346V.

As per the given parameters of the circuit modules the simulation is run for two different cases. The initial SOC of the battery (SOC_{int}) is set with two different values in each case. The SOC_{int}, in one case, is set at 20% when the controller operates in CC mode, and another case, it is set at 90%, it is when the controller switches to CV mode. A comparative analysis is undertaken for these cases with the control module updated with the PR controller. The plotting of the graphs for the given conditions of SOC_{int} is presented with respect to time.

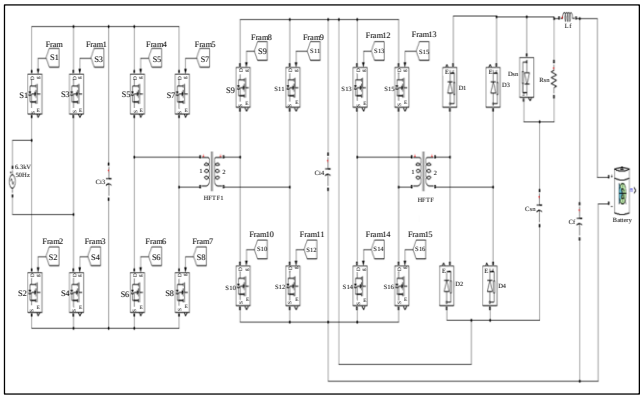

Fig. 5 Simulink model of the proposed EV fast charging station

4.1. Case 1: EV Battery SOC_{int} set at 20%

In this case, the SOC of the EV battery is considered to be 20%, generally considered as low charge. During the condition as the V_{bat} goes below 346V (threshold value) the controller is switched to CC mode. In this mode, I_{ref} = 20A is compared to I_{bat} generating duty ratio for the switches (S1-S4) of the PPC circuit. Below are dynamic graphs noted for the given condition and mode of control.

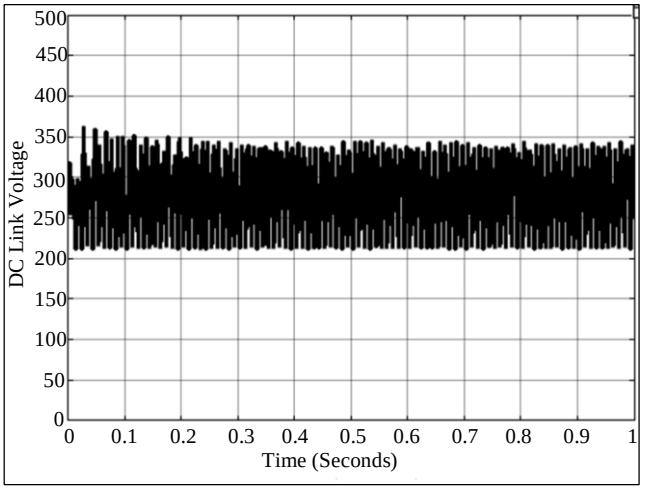

Fig. 6 DC link voltage (input to PPC circuit) for case 1

Figure 6 is the DC link voltage measured (for case 1) at the output of the SST, stepping the voltage from 9kV to 300V. The HFTF causes this vast drop in the voltage with a very low turns ratio of 22.5:1. The ripple in the DC link voltage is caused by the switching of the MOSFETs at a very high frequency. This voltage is input to the PPC circuit charging the EV battery at specified reference values. Figure 7 is the dynamic duty ratio generated by the CC control producing pulses for S1S4 and S2S3.

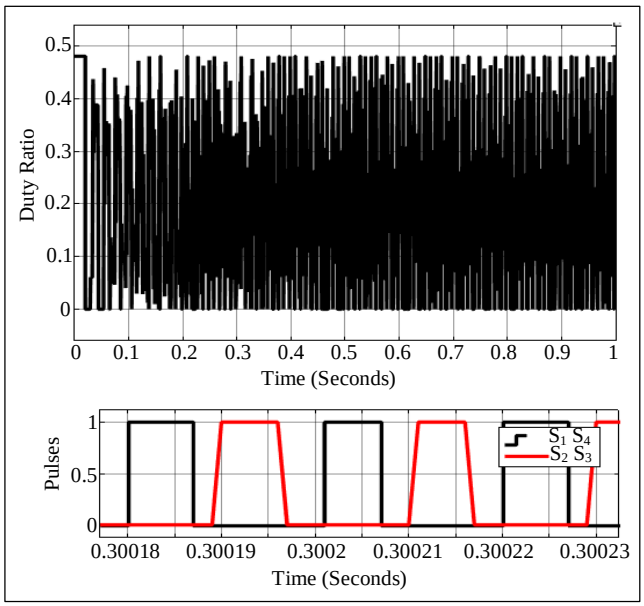

Fig. 7 Duty ratio and gate pulse to the switches for case 1

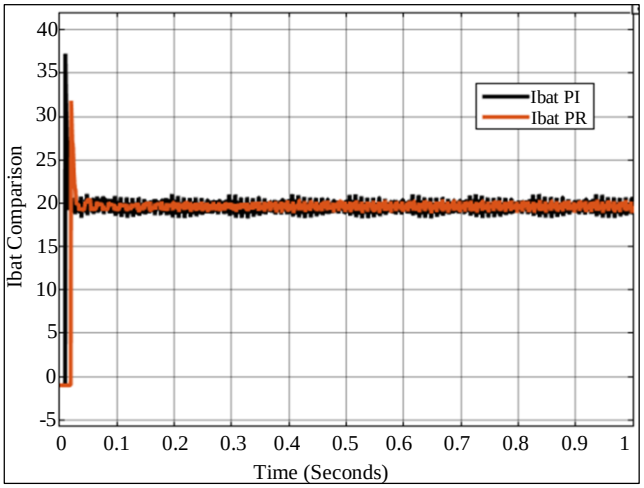

Fig. 8 Battery current comparison for case 1

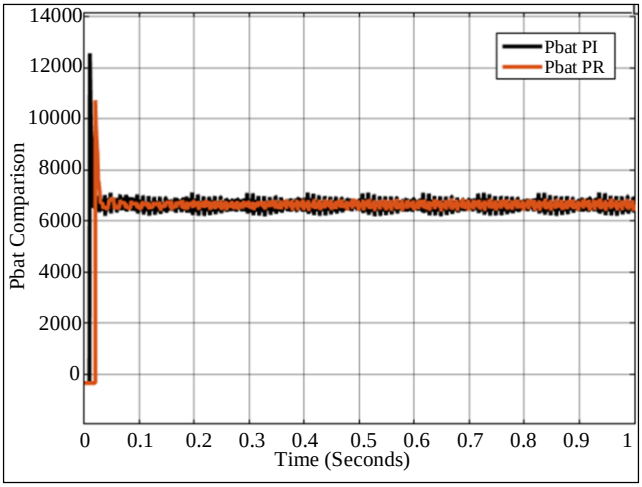

Fig. 9 Battery charging power comparison for case 1

As per the given duty ratio from CC control, the I_{bat} for case 1 is plotted in Figure 8. The graph shows the comparison of I_{bat} with PI and PR controller. As observed, the I_{bat} peak value and ripple are higher for the PI controller as compared to the PR controller. As per the I_{bat} plotting, the P_{bat} also represents the same pattern in Figure 9. A comparison Table 2 is given for the current and power parameters with PI and PR controller operating in case 1.

Table 2. Parameter comparison table for case 1

Name of the Parameter	PI	PR
I_{bat} initial peak	37.2A	31.8A
I_{bat} ripple	15.38%	7.1%
P_{bat} initial peak	12.5kW	10.7kW
P_{bat} ripple	13.5%	6.8%

4.2. Case 2: EV Battery SOC_{int} set at 90%

In this case, 2, the parameters of the complete system are maintained the same but with only a change in the EV battery SOC_{int} value set to 90%. This condition is considered to be an almost full charge, where the intensity of charging needs to be reduced for a healthy battery. As per the given condition, the controller switches to CV mode where the graphs are noted and plotted for the same simulation time.

Figure 10 is the DC link voltage plotted for case 2 which has similar magnitude and ripple content as in case 1. The average magnitude is recorded to be 300V which is the input voltage to the PPC circuit. In Figure 11, the duty ratio for the switches is plotted, generated by CV control as the V_{bat} is above 346V (caused by SOC above 85%).

For case 2 operating in CV mode, the I_{bat} and P_{bat} comparison with PI and PR is shown in Figures 12 and 13, respectively. A comparative parametric Table 3 is given, analyzing the measured results.

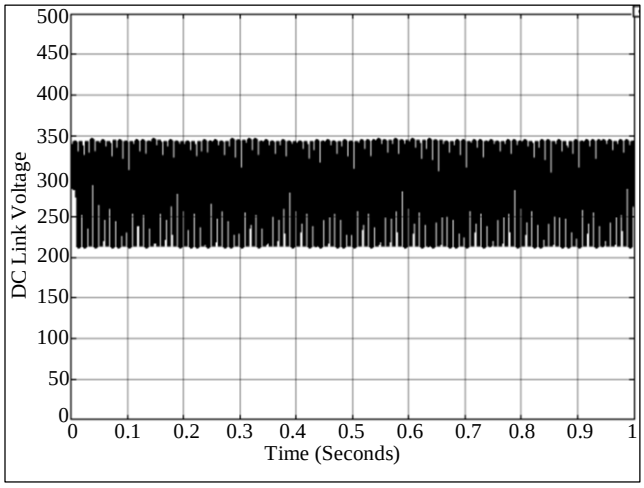

Fig. 10 DC link voltage (input to PPC circuit) for case 2

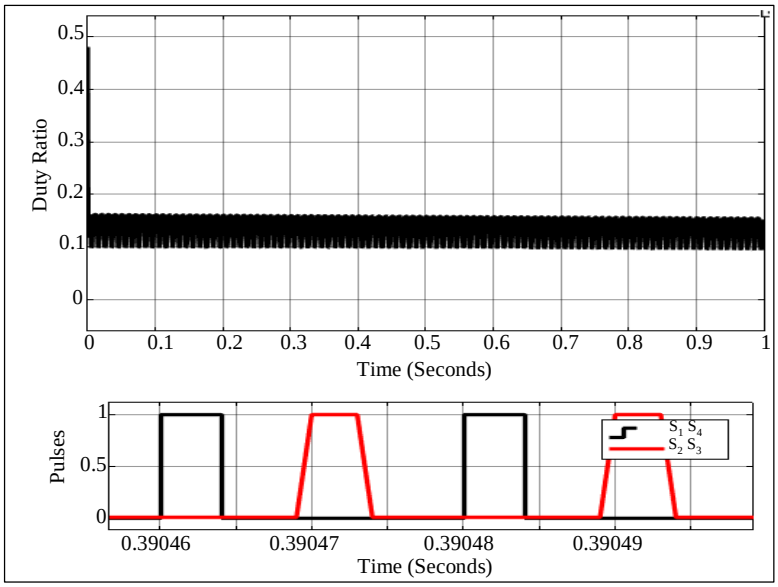

Fig. 11 Duty ratio and gate pulse to the switches for case 2

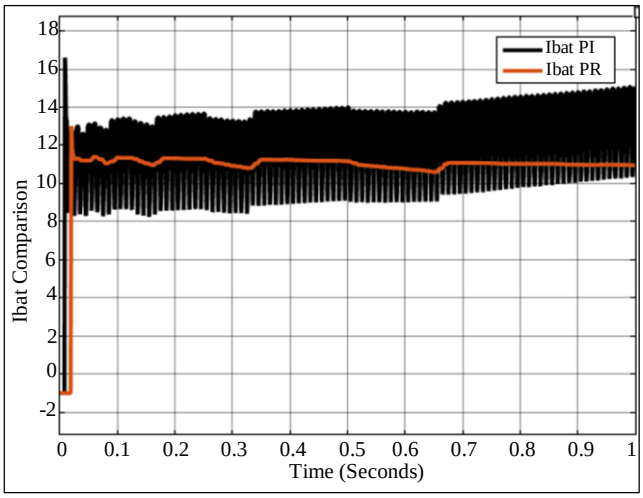

Fig. 12 Battery current comparison for case 2

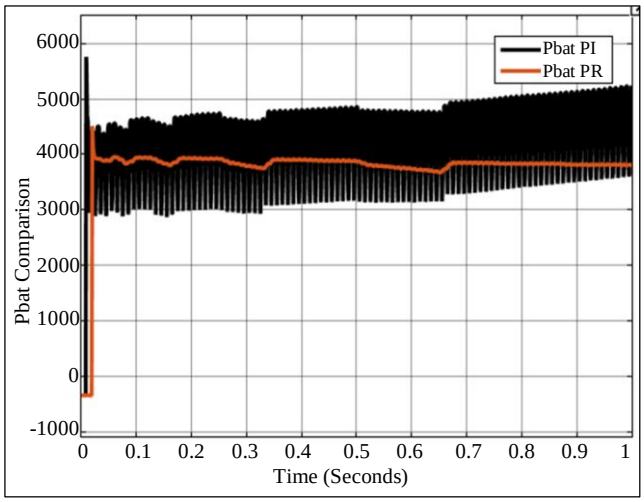

Fig. 13 Battery charging power comparison for case 2

Table 3. Parameter comparison table for case 2

Name of the Parameter	PI	PR
I_{bat} Initial Peak	15.5A	13A
I_{bat} Ripple	16.6%	7.27%
P_{bat} Initial Peak	5.4kW	4.5kW
P_{bat} Ripple	22.2%	6.5%

5. Conclusion

For enhancement of charging heavy EV batteries fast charging method is needed, which can charge with high current amplitude. A partial power charging circuit is designed and modelled for charging the EV battery with high current ratings. For controlling the PPC circuit a CC/CV switcher controlling module is included. The selection of CC/CV modes is considered from the battery voltage feedback compared to the threshold value. In a further modification, the duty ratio generation from the error signals is updated with the PR controller, replacing the conventional PI controller.

The resonance gain (K_r) reduces the ripple in the duty signal, which reduces oscillations in the battery current and charging power. A comparative analysis is carried out with both the PI and PR controllers integrated into the PPC circuit, improving the performance of the circuit topology.

As per the comparative tables for both cases during 20% and 90% SOC_{int} of battery it is observed that the I_{bat} and P_{bat} parameters are improved when the controller is operated with PR controller. The peak value generation and ripple in both parameters are reduced to nearly half with the updated to the charge control.

References

[1] Vishnu Mahadeva Iyer et al., "An Approach towards Extreme Fast Charging Station Power Delivery for Electric Vehicles with Partial Power Processing," *IEEE Transactions on Industrial Electronics*, vol. 67, no. 10, pp. 8076-8087, 2020. [CrossRef] [Google Scholar] [Publisher Link]

[2] IEA, Global EV Outlook 2023, IEA, Paris, 2023. [Online]. Available: https://www.iea.org/reports/global-ev-outlook-2023

[3] U.S. Department of Energy, "*Evaluating Electric Vehicle Charging Impacts and Customer Charging Behaviors-Experiences from Six Smart Grid Investment Grant Projects*," Technical Report, Washington, USA, 2017. [Google Scholar] [Publisher Link]

[4] Mohammed Abdullah Ravindran et al., "A Novel Technological Review on Fast Charging Infrastructure for Electrical Vehicles: Challenges, Solutions, and Future Research Directions," *Alexandria Engineering Journal*, vol. 82, pp. 260-290, 2023. [CrossRef] [Google Scholar] [Publisher Link]

[5] Xiaoou Liu et al., "Dynamic Response Characteristics of Fast Charging Station-EVs on Interaction of Multiple Vehicles," *IEEE Access*, vol. 8, pp. 42404-42421, 2020. [CrossRef] [Google Scholar] [Publisher Link]

[6] Júlio C.G. Justino, Thiago M. Parreiras, and Braz de J. Cardoso Filho, "Hundreds kW Charging Stations for e-Buses Operating under Regular Ultra-Fast Charging," *IEEE Transactions on Industry Applications*, vol. 52, no. 2, pp. 1766-1774, 2016. [CrossRef] [Google Scholar] [Publisher Link]

[7] Jianwei Li et al., "Optimal Design of the EV Charging Station with Retired Battery Systems against Charging Demand Uncertainty," *IEEE Transactions on Industrial Informatics*, vol. 19, no. 3, pp. 3262-3273, 2023. [CrossRef] [Google Scholar] [Publisher Link]

[8] Nima Tashakor et al., "Start-up Circuit for an Electric Vehicle Fast Charger Using SSICL Technique and a Slow Estimator," *IET Generation, Transmission & Distribution*, vol. 14, no. 12, pp. 2247-2255, 2024. [CrossRef] [Google Scholar] [Publisher Link]

[9] Yusuf Yasa, "A System Efficiency Improvement of DC Fast-Chargers in Electric Vehicle Applications: Bypassing Second-Stage Full-Bridge DC-DC Converter in High-Voltage Charging Levels," *Ain Shams Engineering Journal*, vol. 14, no. 9, pp. 1-10, 2023. [CrossRef] [Google Scholar] [Publisher Link]

[10] R. Venugopal et al., "Review on Unidirectional Non-Isolated High Gain DC-DC Converters for EV Sustainable DC Fast Charging Applications," *IEEE Access*, vol. 11, pp. 78299-78338, 2023. [CrossRef] [Google Scholar] [Publisher Link]

[11] Jonatan Rafael Rakoski Zientarski et al., "Series-Connected Partial-Power Converters Applied to PV Systems: A Design Approach Based on Step-Up/Down Voltage Regulation Range," *IEEE Transactions on Power Electronics*, vol. 33, no. 9, pp. 7622-7633, 2018. [CrossRef] [Google Scholar] [Publisher Link]

[12] Jon Anzola, Iosu Aizpuru, and Asier Arruti, "Partial Power Processing Based Converter for Electric Vehicle Fast Charging Stations," *Electronics*, vol. 10, no. 3, pp. 1-16, 2021. [CrossRef] [Google Scholar] [Publisher Link]

[13] J. Rojas et al., "Partial Power DC-DC Converter for Electric Vehicle Fast Charging Stations," *IECON 2017 - 43rd Annual Conference of the IEEE Industrial Electronics Society*, Beijing, China, pp. 5274-5279, 2017. [CrossRef] [Google Scholar] [Publisher Link]

[14] Daniel Pesantez et al., "Transformerless Partial Power Converter Topology for Electric Vehicle Fast Charge," *IET Power Electronics*, pp. 1-13, 2023. [CrossRef] [Google Scholar] [Publisher Link]

[15] Felix Hoffmann et al., "A Multiport Partial Power Processing Converter with Energy Storage Integration for EV Stationary Charging," *IEEE Journal of Emerging and Selected Topics in Power Electronics*, vol. 10, no. 6, pp. 7950-7962, 2022. [CrossRef] [Google Scholar] [Publisher Link]

[16] Li Bao, Lingling Fan, and Zhixin Miao, "Real-Time Simulation of Electric Vehicle Battery Charging Systems," *2018 North American Power Symposium (NAPS)*, Fargo, USA, pp. 1-6, 2018. [CrossRef] [Google Scholar] [Publisher Link]

[17] Wenhao Xiong et al., "A Hybrid Topology IPT System with Partial Power Processing for CC-CV Charging," *IEEE Transactions on Power Electronics*, vol. 39, no. 1, pp. 1701-1712, 2024. [CrossRef] [Google Scholar] [Publisher Link]

[18] Yafei Chen et al., "A Switching Hybrid LCC-S Compensation Topology for Constant Current/Voltage EV Wireless Charging," *IEEE Access*, vol. 7, pp. 133924-133935, 2019. [CrossRef] [Google Scholar] [Publisher Link]

[19] Veli Yenil, and Sevilay Cetin, "Load Independent Constant Current and Constant Voltage Control of LCC-Series Compensated Wireless EV Charger," *IEEE Transactions on Power Electronics*, vol. 37, no. 7, pp. 8701-8712, 2022. [CrossRef] [Google Scholar] [Publisher Link]

[20] Viswaprakash Babu et al., "Power Quality Enhancement Using Dynamic Voltage Restorer (DVR)-Based Predictive Space Vector Transformation (PSVT) with Proportional Resonant (PR)-Controller," *IEEE Access*, vol. 9, pp. 155380-155392, 2021. [CrossRef] [Google Scholar] [Publisher Link]

[21] Mohammad Parvez et al., "Comparative Study of Discrete PI and PR Controls for Single-Phase UPS Inverter," *IEEE Access*, vol. 8, pp. 45584-45595, 2020. [CrossRef] [Google Scholar] [Publisher Link]

[22] Santanu Kumar Dash, and Pravat Kumar Ray, "Power Quality Improvement Utilizing PV Fed Unified Power Quality Conditioner Based on UV-PI and PR-R Controller," *CPSS Transactions on Power Electronics and Applications*, vol. 3, no. 3, pp. 243-253, 2018. [CrossRef] [Google Scholar] [Publisher Link]